Carbohydrate Polymers 111 (2014) 333–347

Contents lists available at ScienceDirect

Carbohydrate Polymers

journal homepage: www.elsevier.com/locate/carbpol

Effect of spatial distribution of wax and PEG-isocyanate on the morphology and hydrophobicity of starch films

Delina Muscat[a], Raju Adhikari[b], Mark J. Tobin[c], Stafford McKnight[d], Lara Wakeling[a], Benu Adhikari[e,*]

[a] School of Health Sciences, University of Ballarat, VIC 3353, Australia
[b] Materials Science and Engineering, CSIRO, Clayton South, VIC 3169, Australia
[c] IR Beamline, Australian Synchrotron, Clayton, VIC 3168, Australia
[d] School of Science, Information Technology & Engineering, University of Ballarat, VIC 3353, Australia
[e] School of Applied Sciences, RMIT University, Melbourne City Campus, VIC 3001, Australia

ARTICLE INFO

Article history:
Received 6 January 2014
Received in revised form 17 April 2014
Accepted 18 April 2014
Available online 29 April 2014

Keywords:
Amylose
Natural wax
Hydroxyl-PEGylation
Synchrotron-based FTIR
Hydrophobicity
Surface morphology

ABSTRACT

This study proposes a novel method for improving surface hydrophobicity of glycerol plasticized high amylose (HAG) films. We used polyethylene glycol isocyanate (PEG-iso) crosslinker to link HAG and three natural waxes (beeswax, candelilla wax and carnauba wax) to produce HAG + wax + PEG-iso films. The spatial distributions of wax and PEG-iso across the thickness of these films were determined using Synchrotron-based Fourier transform infrared spectroscopy. The hydrophobicity and surface morphology of the films were determined using contact angle (CA) and scanning electron microscopic measurements, respectively. The distribution patterns of wax and the PEG-iso across the thickness of the film, and the nature of crystalline patterns formed on the surface of these films were found to be the key factors affecting surface hydrophobicity. The highest hydrophobicity (CA >90°) was created when the PEG-iso was primarily distributed in the interior of the films and a hierarchical circular pinnacle structure of solidified wax was formed on the surface.

1. Introduction

To improve water barrier and water repelling properties in starch films, lipids are introduced to the starch film composition as they possess low surface energy and high hydrophobicity (Han & Gennadios, 2005). When combining lipids with starch and other hydrophilic plasticizers their immiscibility is the main limitation. To overcome this problem several approaches have been utilized for incorporating lipids into the films. These approaches can be categorized as: blending; physisorption and chemisorption (Pereira, Paulino, Rubira, & Muniz, 2010).

In recent years many advances have been made in modifying the physicochemical characteristics of starch to avoid its limitations in hydration, swelling, granule rupture, viscosity and cohesiveness (Tezcaner & Hasirce, 2004). Such modification of starch improves a number of functional properties which cannot be obtained from its native state. Modification is a process of altering the starch structure by affecting the hydrogen bond in a controllable manner. Such modification alters the form/shape of the granule and composition of amylose molecules (Iheagwara, 2013; Yiu, Loh, Rajan, Wong, & Bong, 2008). One of these advances is the "grafting-to" approach of starch through chemical modifications with other polymers, such as polyethylene glycol (PEG). The covalent bonding between starch and PEG represents a logical approach for modifying the surface properties of the starch, allowing the bulk composition to remain unchanged, whilst the modified surface provides desired functionality (Rhodes, Sandhu, & Onis, 2011). Modification of hydroxyl groups of starch has gained much attention as hydrophobic substances can be attached to starch molecules by using spacers or functionalized amphiphilic macromolecules (FAMs). This attachment (of FAMs) alters the fundamental properties and the conformation and structure of starch (de Vlieger, 2003). The spacer helps reduce the steric hindrance to the activity of the attached compound (Weetall, 1993). PEG is neutral and it has very low reactivity unless modified with functional groups (such as hydroxyl, carboxyl, esters, amides, etc.) therefore does not disrupt the structure of attached starch molecules. The amphiphilic (i.e. molecule containing hydrophilic and hydrophobic moieties) part of the PEG contains two ends (α-end and the ω-end) which provide a ready site for covalent attachment to other molecules and surfaces (Harris, 1992). These two ends can carry the same or different functional groups (Kumar, Prakash, Laxmi, & Krishma, 2011). Thus PEG

* Corresponding author. Tel.: +61 3 992 59940; fax: +61 3 992 53747.
E-mail address: benu.adhikari@rmit.edu.au (B. Adhikari).

http://dx.doi.org/10.1016/j.carbpol.2014.04.072
0144-8617/

can be an ideal molecule in attaching wax to a starch matrix. Modification of starch surface can be achieved by using chemisorption techniques. Chemisorption involves a covalent linkage between a polymer chain and a surface. The chemical modification processes where the polymer chains can be covalently grafted (i.e. attached) to the surface of the substrate can utilize the "grafting-to" approach.

This study considers the "grafting-to" approach where polymers are anchored onto the surface via chemical bonds formed between reactive groups on the surface and reactive end-groups on the polymer backbones (Brittain & Minko, 2007; Ruhe, 2004). This approach aims to attach polymers to a surface using a system where the polymer carries an "anchor" or a 'functional' group either as an end group or in a side chain. A functional group can be reacted with appropriate sites at the substrate surface, thus yielding a surface-attached monolayer of polymer molecules. The "grafting-to" approach generates so-called "polymer brushes" or FAMs, which are assemblies of long-chain polymers (e.g. PEG) attached by one end to a support and extended from the surface (Fink, 2011). The introduction of a variety of functional groups has made polymer brushes attractive for fabrication of surfaces with a controlled wettability (Chechik, Crooks, & Stirling, 2000).

The PEG has been considered as a viable chemical to act as a FAM or to synthesize a FAM from it. It is a linear or branched polyether terminated with hydroxyl groups, with a general structure of [HO-(CH_2CH_2O)n CH_2CH_2-OH]. It is a water-soluble, amphiphilic, nontoxic polyether exhibiting almost no reactivity unless modified with functional groups. The two terminal hydroxyl groups of the PEG molecules provide a ready site for covalent attachment to other molecules and surfaces since the polyether backbone is quite chemically inert (Borona & Drioli, 2009; Harris, 1992). These terminal hydroxyl groups enable PEG to be used as a spacer moiety or linker where they are converted to reactive functional groups. The PEG functional groups are synthesized through chemical modification of PEG's terminal hydroxyl groups through the substitution of hydroxyl group by one or more functional groups. The reactive functional group of activated PEG can then be attached to a specific site on the surface of the compound (e.g. starch and wax).

In order to couple the PEG chains onto different macromolecules, such as starch and natural waxes, it is necessary to have PEG activated with a functional group at one end or both ends of the termini. The choice of the functional group depends on its specific functionality and its ability to couple with the PEG (Torchilin, 2010), natural wax and starch molecules. A study by Lin, Huang, Chang, Anderson, & Yu (2011) demonstrated how starch nanocrystals could be modified by hydroxyl-PEGylation between hydroxyl groups (—OH) and isocyanate groups (—NCO). This surface chemical modification weakened the polarity of the original starch nanocrystals by decreasing the hydrophilicity, proportion of polar components and surface energy.

A novel method based on the "grafting-to" approach has been attempted in which the PEG is grafted to the surface of starch using different coupling agents. The OH groups of PEG are endcapped with isocyanate (—NCO) functional groups to form PEG-isocyanate (PEG-iso). This PEG-iso is best suited for hydroxyl containing matrices (Prajapati, Patel, & Patel, 2011) such as starch (Veronese, 2001) in producing a urethane linkage (Hermanson, 2008) which is referred to as hydroxyl PEGylation. Starch has many hydroxyl groups on its chains (three hydroxyl groups at C-2, C-3, and C-6) and all of these groups can be modified by introducing PEG–isocyanate molecules.

The natural waxes available in the cuticle of higher plants determine their hydrophobic characteristics. According to Ensikat, Boese, Mader, Barthlott, & Koch (2006) and Jetter and Kunst (2008) plant epicuticular and cuticular waxes are complex mixtures of relatively non-polar long-chain aliphatic compounds. These compounds are characterized by unbranched, fully saturated hydrocarbon backbones which include alkanes and their derivatives. These waxes consist of a primary oxygen-containing functional group such as hydroxyl (—OH), carbonyl (—CO) or carboxyl (—COOH). Therefore, plant waxes are typically mixtures of primary alcohols, ketones, aldehydes and fatty acids, as well as alkanes with chain lengths ranging from 20 to 40 carbons. These long-chain aliphatic compounds such as alkanes and hydrocarbons either lack functional groups or have primary functional groups such as very-long-chain fatty acids, aldehydes and primary alcohols. Plant cuticular wax constituents have secondary functional groups which mostly consist of a combination of hydroxyl and carbonyl functional groups. The presence of these functional groups in these natural waxes provides some insight regarding what FAM to use. The FAMs such as PEG-isocyanate (Prajapati, Patel, & Patel, 2011) can be used to react with hydroxyl groups to produce a chemical linkage between wax and starch.

As explained above, both starch and natural wax have hydroxyl groups present in their structure, thus PEG-isocyanate can be used as a linker (i.e. urethane linkage) between these two biopolymers. In the hydroxyl-PEGylation process, the urethane linkage is produced when a chemical reaction occurs between an isocyanate (NCO groups) and alcohol (OH groups). Aliphatic diisocyanates are preferred to produce the urethane linkage as they are capable of reacting with most compounds containing active hydrogen, such as alcohols (Howard, 2002). This is where the functional group of isocyanate (NCO groups) and alcohol (OH groups) rearrange. More specifically, the hydrogen atom of the hydroxyl group is transferred to the nitrogen atom of the isocyanate. The end-product of the hydroxyl-PEGylation reaction is PEG-isocyanate (PEG-iso) which is used for hydroxyl group conjugation in yielding a stable urethane linkage. PEG-iso is then used to attach the hydroxyl group containing matrices, such as starch and lipid, together.

The surface modification of starch exhibits a distinctive structure depending on the interaction of components present in the structure. The molecular vibration of each functional group of each macromolecule present in the modified starch structure can be identified using Fourier transform infrared spectroscopy (FTIR). Under FTIR these functional groups produce unique bands which enable components to be identified in the starch matrix. The relatively unique absorption of lipid vibrations usually are located at 2800 cm^{-1} to 3000 cm^{-1} as antisymmetric and symmetric stretching vibrations of CH_3 (ca. 2961 cm^{-1} and 2871 cm^{-1}) and CH_2 (ca. 2925 cm^{-1} and 2853 cm^{-1}) groups of acyl chains. In addition, strong bands at 1738 cm^{-1} stretching vibration arise from the carbonyl ester C=O band (Yu, 2012, 2004). The IR spectral features of corn starch consists of its major absorption peaks between 3000 cm^{-1} and 3600 cm^{-1} due to OH stretching (Coates, 2000; Zhang & Han, 2006). The sharp peak at 2924 cm^{-1} is characteristic of CH_2 stretching (Park, Im, Kim, & Kim, 2000). The peak occurring at 1641 cm^{-1} is associated with the tightly bound water present in the starch (Zhang & Han, 2006) due to the hygroscopic nature of starch. The peaks at 1409 cm^{-1} and 1433 cm^{-1} are related to the CH_2 bending. The PEG-iso produces an increase in the relative intensity of the urethane band with respect to that of C=O stretching of the overlapping carbonyl groups associated with hydrogen bonds of the urethane linkage at 1732 cm^{-1} and a NH urethane band (3300 cm^{-1}) which overlaps over the OH band. The broad peaks at 2940 cm^{-1} and 2878 cm^{-1} correspond to antisymmetric and symmetric CH_2 stretching vibrations, respectively. Another distinctive absorbance band for PEG-iso is associated with carbonyl coupled with N-H bending vibrations producing a peak at 1540 cm^{-1} (Guelcher et al., 2005). These unique IR spectra of starch, wax and PEG-iso will assist in the characterization of composite films through the evaluation of interactions between the film components.

The Synchrotron-based Fourier transform infrared spectroscopy (S-FTIR) is capable of providing important information such as distribution of chemical constituents and functional groups of wax and PEG-iso across the thickness of the starch-wax composite films. This information helps to gain fundamental understanding of how chemical functional components are distributed at micron level in the films produced through oil-in-water (O/W) emulsion method (Muscat, Adhikari, McKnight, Guo, & Adhikari, 2013). The mapping capability of S-FTIR simultaneously provides both the morphological and chemical information within these composite films.

To date there has been no application of S-FTIR mapping to investigate the structural feature and the distribution of natural wax in HAG films produced using the 'grafting to' method. The S-FTIR mapping is also capable of proving understandings on the structural–chemical features created due to the interactions among the components (such as wax, amylose–glycerol matrix, water and PEG-isocyanate) of the composite films.

Although hydrophobicity can be introduced on a film surface by the addition of wax, the increase in surface texture (or roughness) due to the formation of epicuticular wax crystals on the film surface can achieve a greater degree of hydrophobicity. It has been shown that a particularly formed micro-roughness assists in creating a high level of water repellency of surfaces (Muscat, Adhikari, McKnight, Guo, & Adhikari, 2013; Wagner, Furstner, Barthlott, & Neinhuis, 2003). These superhydrophobic surfaces have characteristic CA value (of water) higher than 150°. In nature, this phenomenon is commonly known as "lotus effect", where the surface of the lotus leaf has the characteristic superhydrophobicity and self-cleaning. The lotus plant demonstrates such systems with the combination of papillose epidermal cells coated with tubular epicuticular wax crystals hierarchically structured (Koch & Ensikat, 2008; Marmur, 2004) to the cuticle. The wax crystals, which are composed of hydrophobic substances, provide a water repellent layer and with the combination of the micron scale surface roughness, facilitate water to form a spherical droplet at the tip the wax structure (Oles, Nun, Dambacher, & Schleich, 2000). The surface nano-topography reduces the number of available contact points between the leaf and water droplets sitting on it causing water beads to form and roll off the leaf. In general, lotus effect is achieved when the surface is covered with a low surface energy material, such as wax, which has a fine structure. The surface texture allows the capture of air bubbles in the area between the water and substrate and thus prevents their contact. Therefore, the surface morphology of the film surface will have to be given attention while investigating the surface roughness formed by any method applied to develop such wax–starch films.

The objective of this study was to apply S-FTIR 2D mapping to determine the distribution of wax, and PEG-iso within high amylose glycerol (HAG)-wax films produced by the 'grafting to' technique. By using S-FTIR mapping the functional groups of these macromolecules can be identified and their concentration profiles can be mapped within these films. This method may offer considerable new insight into the interaction and distribution of the wax and PEG-iso linker within the starch matrix as a function of concentration of natural waxes and PEG-iso. The S-FTIR 2D imaging data are compared with the contact angle data and scanning electron microscope (SEM) micrographs of these films to correlate the distribution of wax on the film surface with the measured film hydrophobicity.

2. Materials and methods

2.1. Materials

High amylose (HA) corn starch (Gelose 80) containing 70–80% (w/w) amylose was purchased through Penfords (Australia) and constituted the continuous matrix of films. Glycerol (G) was used as a plasticizer and was purchased from Consolidated Chemical Company (Melbourne, Australia). The natural waxes, i.e. beeswax (BW), candelilla wax (CL) and carnauba wax (CB), were purchased from New Directions Aromatics Inc. (Australia). The Certificate of Analysis of these waxes was provided by this company. The PEG (MW 600), dibutyltin dilaurate (95%, DBTDL) and 1,6-diisocyanatohexane (98%, HDI), were purchased from Sigma–Aldrich, and were used without further purification. All the materials were used as received and the moisture content of the raw materials was compensated while preparing the slurry mixture for gelatinization.

2.2. Methods

2.2.1. Synthesis of PEG-isocyanate

A standard bulk method was used to synthesize PEG-isocyanate, where PEG 600 (average molecular weight 570–630, 8.33×10^{-2} mol) was reacted with HDI (16.6×10^{-2} mol) (1:2) in a triple-neck round-bottom glass reactor in the presence of dibutyltin dilaurate (0.2% DBTDL) catalyst. The round-bottom glass reactor was equipped with a thermometer, nitrogen purging hose and a reflex condenser. The mixture was stirred and heated on an oil bath equipped with a temperature controlling mechanism at 70 °C for 120 min under nitrogen atmosphere. The completion of the reaction was monitored by FTIR by the disappearance of NCO peak at 2210 cm^{-1}. The final product, PEG-isocyanate, was stored in an air tight container at 4 °C.

2.2.2. Preparation of the suspension

HA and G (80:20, w/w) were added to distilled water maintaining a total solid concentration of 5% (w/w). This HA:G ratio was maintained to produce good flexible films as reported in our previous study (Muscat, Adhikari, Adhikari, & Chaudhary, 2012). The HAG suspension was gelatinized using a high temperature-high pressure stirred laboratory autoclave (Amar Equipment Company, Mumbai, India) with an inbuilt overhead stirrer fitted to a 6 bladed pitch blade turbine. The HAG suspension was gelatinized at 140 °C using 500 rpm agitator speed. The suspension was held for 30 minutes at 140 °C before cooling down to below 100 °C.

2.2.3. Preparation of HAG + wax dispersions

While maintaining a temperature above 85 °C using a hot plate (Framo Geratechnik, Germany) the molten wax was added to the fully gelatinized HAG dispersion and thoroughly stirred. The beeswax (BW), candelilla wax (CL) and carnauba wax (CB) were added individually to the HAG suspension at two different concentrations of 5% (w/w) and 10% (w/w). To ensure a thorough mixing of molten wax droplets within the HAG dispersion, coarse homogenization with a high-shear mixer (Ultra-Turrax, Model T25, IKA-Works, USA) was performed at 15,000 rpm for 3 minutes followed by 22,000 rpm for 1 minutes.

2.2.4. Preparation of HAG + wax + PEG-isocyanate dispersions

Melted PEG-isocyanate was added at different concentrations of 1%, 5% and 20% (w/w) to the HAG + wax solution and thoroughly mixed using the high-shear mixer (Ultra-Turrax, Model T25, IKA-Works, USA) at 15,000 rpm for 3 min.

2.2.5. Film casting and conditioning

The HAG + wax and HAG + wax + PEG-isocyanate films were prepared by syringing 10 mL of the dispersions into plastic polystyrene dishes with a 90 mm diameter. Films were dried for 24 h at 20 ± 1 °C, in an air conditioned room. These films were stored in a desiccator containing magnesium nitrate (52.9% RH (a_w = 0.529) at 20 ± 1 °C) for at least 48 h for conditioning before analysis.

2.2.6. Determination of interaction amongst the film components

To identify the specific spectral "signatures" of the natural waxes, such as BW, CL and CB solid samples of each wax, HAG and PEG-iso were analyzed by FTIR spectroscopy. The specific spectral "signatures" of these raw materials were determined by a universal attenuated total reflectance (UATR) FTIR spectrometer (Perkin Elmer, Frontier™, USA) with a diamond coated zinc selenide crystal plate (reflection plate with pressure arm). Perkin-Elmer spectrum software (version 6.3.4) was used for FTIR analysis. The spectra were obtained in between 1000 cm^{-1} and 4000 cm^{-1} wavenumbers at 4 cm^{-1} step.

2.2.7. Preparation of film samples for S-FTIR microspectroscopy

Sections of the film samples were inserted between two polystyrene portions to establish a firm assembly for cutting as described in Muscat, Tobin, Guo, & Adhikari (2014). The embedded film samples were cut into thin cross-sections (ca. 8 μm thick) using a rotary microtome (4060RE, Triangle Biomedical Sciences, Inc., USA) at Australian Synchrotron's facility (Clayton, VIC, Australia) 24 h prior to analysis. The cross-sections were mounted onto CaF_2 windows (size: 13 × 1 mm disc; Cyrstran Limited, UK) for S-FTIR analysis in transmission mode.

2.2.8. Analysis of molecular spectral data and imaging of molecular chemistry

The S-FTIR measurements were performed on the FTIR beamline at the Australian Synchrotron's facility (Clayton, VIC, Australia). Spectra were collected with a Bruker Hyperion 2000 IR microscope (Bruker Optik Gmbh, Ettlingen, Germany) equipped with a liquid nitrogen cooled HgCdTe (MCT) detector with a 36× IR objective. The Hyperion 2000 microscope was coupled to a Bruker Vertex 80 spectrometer. Spectral maps and line scans were collected in transmission mode by scanning the computer-controlled microscope stage at an aperture of 5 μm × 5 μm, and an *X*–*Y* spatial step size of 2 μm.

The spectral data of the films were collected in the mid-IR range 4000–1100 cm^{-1} using a CaF_2 window (Miller, 2002), at a resolution of 4 cm^{-1} with 64 scans co-added. The stage control, data collection and the background correction of spectra were performed using Opus 6.5 (Bruker, Optik Gmbh, Ettlingen, Germany) software version 2.0. Data was saved as Opus Spectrum files for single spectrum and Opus Multiple files for 2D IR map files. Opus Multiple files contained all the spectral and *X*–*Y* spatial information for a two-dimensional grid map and the captured images. Opus 7.0 (Bruker, Optik Gmbh, Ettlingen, Germany) software equipped with video mapping, was used to generate and analyze 2D absorbance maps and the data was converted to 2D chemical maps.

2.2.9. Determination of wax and PEG-iso distribution in the films

Spectra of the natural waxes were analyzed by the UATR FTIR spectrometer to identify functional groups present in these waxes (Muscat, Tobin, Guo, & Adhikari, 2014). The most intense vibrations in the infrared spectra of lipid systems are the CH_2 stretching vibrations region. The antisymmetric and symmetric stretching of CH_2 was observed at 2916 cm^{-1} and 2840 cm^{-1}, respectively. These two bands are considered to be the strongest bands in lipid spectra and are associated with the presence of alkanes (Stuart, 2004). Furthermore, a peak at 2840 cm^{-1} was observed in the spectra of natural waxes but not in that of HAG or PEG-iso (Fig. 1A). Therefore, by selecting the 2840 cm^{-1} wave number in the HAG + wax + PEG-isocyanate films the wax distribution can be determined across the thickness of these films. The wave number 1530 cm^{-1} corresponds to a carbonyl vibration coupled with NH bending and was subsequently used to determine the distribution of PEG-isocyanate in these films (Fig. 1A). To generate S-FTIR maps the integrated area of the antisymmetric CH_2 and NH peaks at 2840 cm^{-1} and 1530 cm^{-1}, respectively, was calculated for each pixel within each data set with the integration calculated above the baseline between two points on the spectral curves at 2860 cm^{-1} and 2830 cm^{-1} for CH_2 and 1560 cm^{-1} and 1500 cm^{-1} for NH.

The chemical intensity scale displays a range of colours from blue to pink or white to make it easier to interpret the distribution of wax and PEG-iso across the films under peaks centred at 2840 cm^{-1} (CH_2 stretching) and 1530 cm^{-1} (NH bending), respectively. As shown in Figs. 2–5 the blue suggests the absence of these components, while pink and/or white denotes the presence of these components at a higher proportion. From these chemical intensity scales it is possible to reveal the pattern of wax and PEG-iso distribution within these films.

2.2.10. Contact angle

The contact angle (CA) is the most commonly used measure of wettability or surface hydrophobicity. The static sessile drop method determines the angle formed at the interface and surface tension between the solid-liquid surrounded by air and was used to determine the contact angle of the HAG + wax + PEG-isocyanate films. An apparatus consisting of a stereomicroscope (Zeiss, Carl Zeiss Microscopy GmbH, Germany) connected to a high-resolution digital camera (EOS 60D, Canon, USA) was used. Software to capture the digital image was part of the camera hardware and images were captured into a personal computer. A horizontal beam held the microscope parallel to the surface and was positioned on a three-axis moving platform. To provide lighting, a bank of LEDs was mounted behind the sample holder with a white background (Muscat, Adhikari, McKnight, Guo, & Adhikari, 2013).

The film was mounted to a stainless steel block with double sided tape. The drop (7 μL) of Milli-Q water was carefully placed on the horizontal surface of the film with the aid of an auto pipette (Finnpipette, 0.5–10 μL). The CA values were determined using ImageJ programme (Rasband, 2012) with the plug-in for measuring CA (Brugnara, 2006). The plug-in programme fits the profile of the drop using an edge detection algorithm to find the drop edge (Williams et al., 2010) and calculates the contact angle using the sphere approximation or the ellipse approximation. In our study, the Both BestFits selection gave consistent results for contact angles >30° and the Sphere selection was used for drops with contact angles <30° (Brugnara, 2006; Williams et al., 2010). The reported contact angle values are the mean value of five measurements taken at a minimum of four different positions on the film.

2.2.11. Determination of morphological features of the films

Film surface topography was examined by scanning electron microscopy (SEM, JEOL-JSM 6300, Japan). Film was mounted onto a double sided adhesive carbon tape set on aluminium stubs, which were coated with gold under vacuum. The gold coated samples were analyzed at 5 kV, 300× and 3000× magnification to obtain 100 μm and 10 μm micrographs, respectively in order to allow better observation of the surface morphology of the films. The HAG and HAG + wax films were tilted at an angle of 25° in order to obtain a better image of the cross section of the films.

2.2.12. Statistical analysis

The surface hydrophobicity or contact angle related measurements were performed at least in triplicate and the mean values are reported. The SPSS statistical package (Version 21, Lead Technologies, USA) was used for analysis of variance (ANOVA) to determine whether or not significant difference existed between two mean values. A confidence level of 95% ($p < 0.05$) was used and Paired-samples *T* test was used in these calculations.

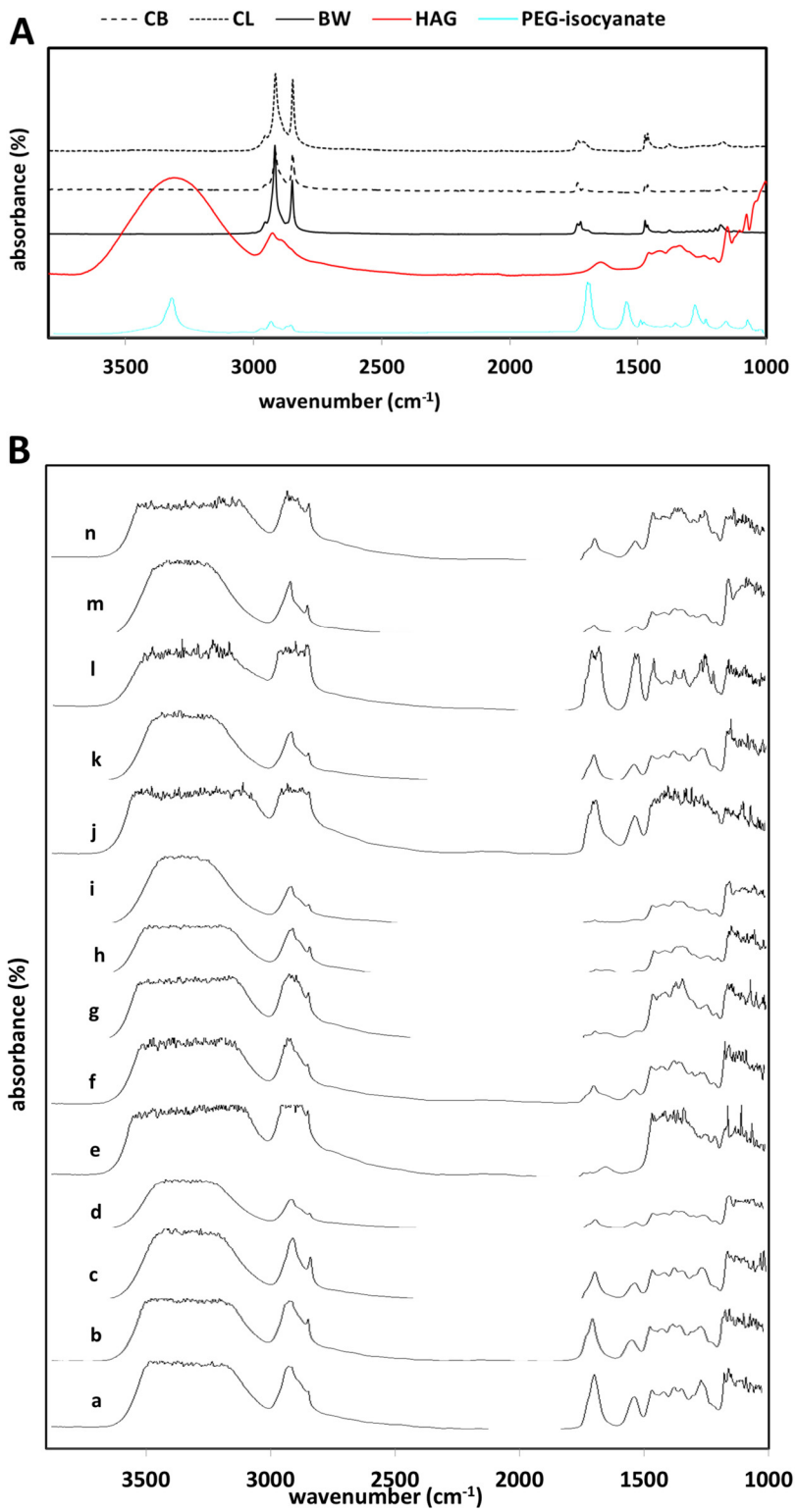

Fig. 1. The FTIR spectra of raw materials (A) carnauba wax, candelilla wax, beeswax, HAG and PEG-iso and the HAG + WAX + PEG-iso films (B) HAG + 5% CB + 20% PEG-iso (a), HAG + 5% CL + 20% PEG-iso (b), HAG + 5% BW + 20% PEG-iso (c), HAG + 5% CB + 5% PEG-iso (d), HAG + 5% CL + 5% PEG-iso (e), HAG + 5% BW + 5% PEG-iso (f), HAG + 5% CB + 1% PEG-iso (g), HAG + 5% CL + 1% PEG-iso (h), HAG + 5% BW + 1% PEG-iso (i), HAG + 10% CB + 20% PEG-iso (j), HAG + 10% CL + 20% PEG-iso (k), HAG + 10% BW + 20% PEG-iso (l), HAG + 5% CL + 5% PEG-iso (m), HAG + 5% BW + 5% PEG-iso (n).

3. Results and discussion

Each of the components of HAG + wax + PEG-iso film has its own vibrational "fingerprints" with characteristic absorption and relative intensity, as shown in Fig. 1A. The natural waxes were readily identified through the spectral features associated with their characteristic functional groups, as stated in Muscat, Tobin, Guo, & Adhikari (2014). The characteristic wavenumber indicating the presence of natural wax is CH_2 stretching (2840 cm^{-1}). Similarly, the wavenumber indicating the presence of PEG-isocyanate is

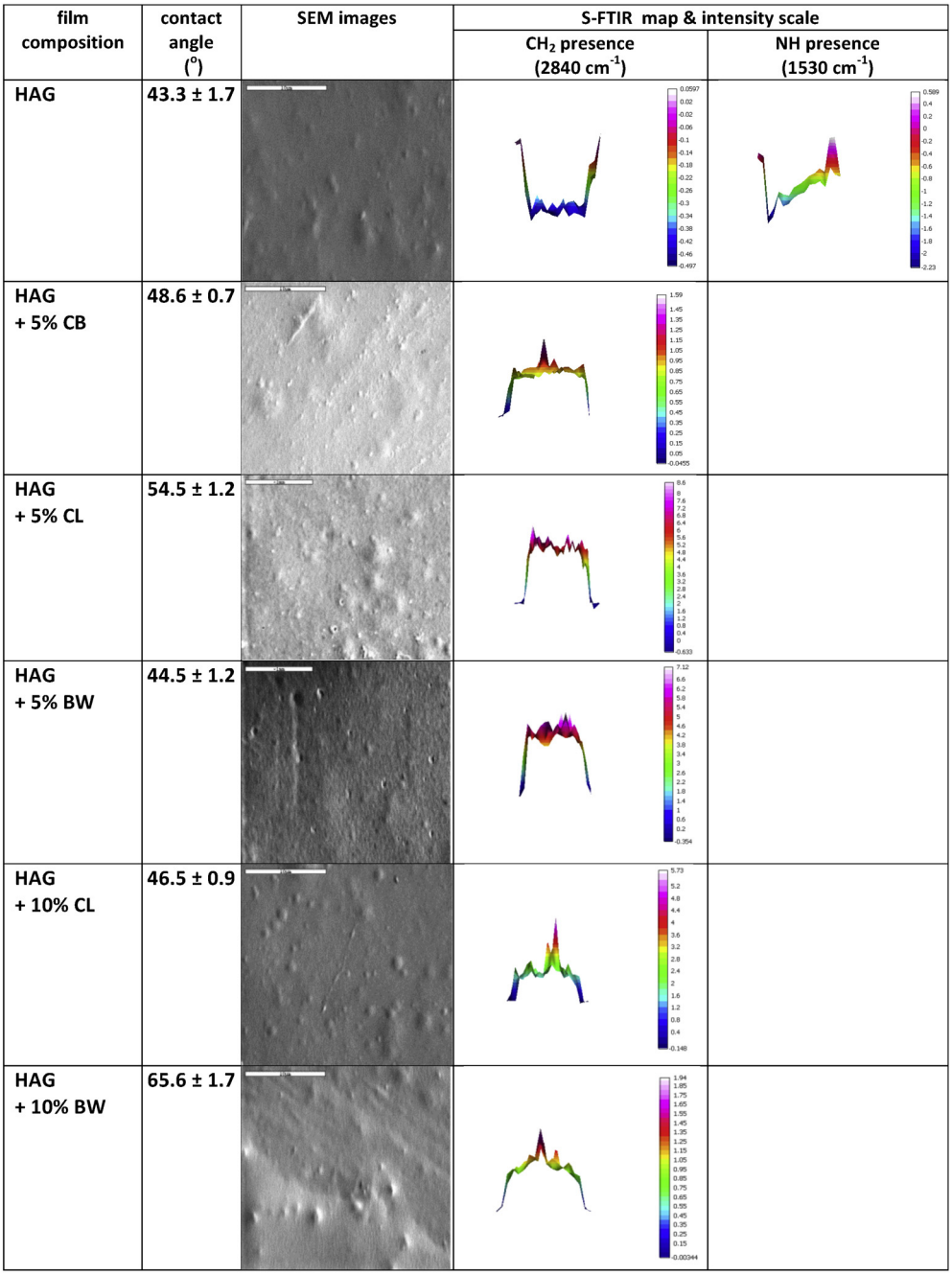

Fig. 2. SEM images (at 10 μm) and CA values of HAG, HAG + 5% wax, and HAG + 10% wax films. The S-FTIR maps indicate the presence of wax and PEG-isocyanate by CH_2 and NH absorption intensity colour coded scales, respectively, across the thickness these films. (The S-FTIR map and SEM image of HAG + 10% CB film are not included due to wax separation during drying.) (For interpretation of the references to color in this figure legend, the reader is referred to the web version of the article.)
Some of the SEM images and CA values are adapted from Muscat, Tobin, Guo, & Adhikari (2014).

1530 cm^{-1}, which originates from the NH bending vibration of the urethane bond present in the PEG-isocyanate linker. The absence of an NCO peak from 2250 cm^{-1} to 2270 cm^{-1} in the PEG-iso spectrum indicated that the reaction between 1,6-diisocyanatohexane (HDI) and poly(ethylene glycol) (PEG) in the presence of a tin catalyst (dibutyltin dilaurate) proceeded to complete conversion (Guelcher et al., 2005; Roizard, Nilly, & Lochon, 2001). The formation of hydrogen bonding in the urethane linkage is indicated by the appearance of C=O peak at 1730 cm^{-1}. Consequently, the appearance of peak 1730 cm^{-1} and absence of peak 2210 cm^{-1} indicate 100% reaction efficiency.

3.1. Evidence of grafting

The extent of crosslinking of PEG-iso with the starch component of HAG + wax films was analyzed by using FTIR. Fig. 1B presents the FTIR spectra of the HAG + wax + PEG-iso films. When PEG-iso is added in the HAG + wax dispersion, it preferentially reacts with the OH groups of starch rather than reacting with the hydrophobic wax. The characteristic urethane peak corresponding to the carbonyl vibration coupled with NH bending (C—N—H urethane), C—N stretching, N—H (symmetrical bending) at wave number 1530 cm^{-1} in the finger print region has confirmed the

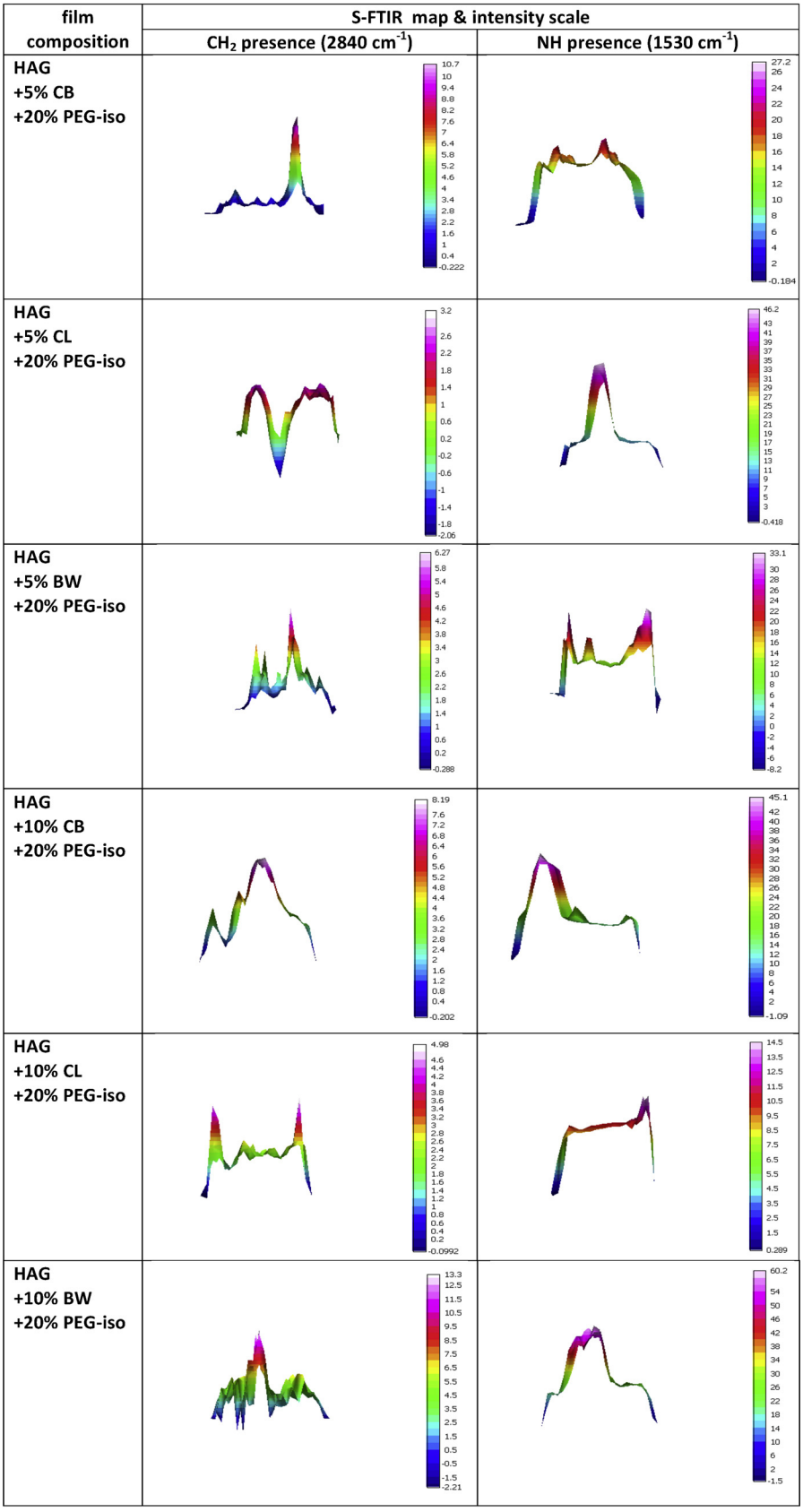

Fig. 3. The S-FTIR maps of HAG + 5% wax + 20% PEG-iso and HAG + 10% wax + 20% PEG-iso films. These S-FTIR maps indicate the presence wax and PEG-isocyanate by CH_2 and NH absorption intensity colour coded scales, respectively, across the thickness of these films. (For interpretation of the references to color in this figure legend, the reader is referred to the web version of the article.)

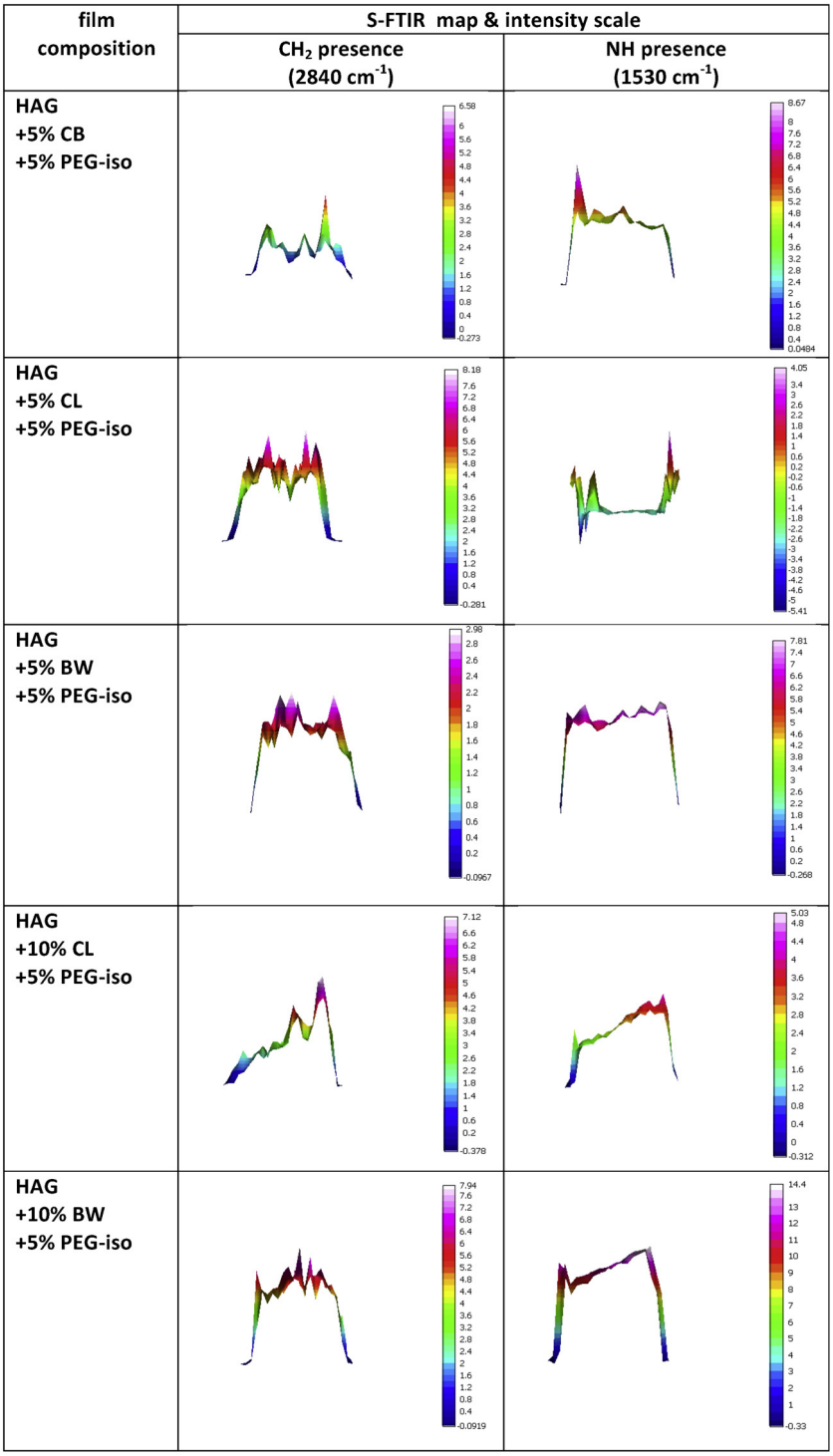

Fig. 4. The S-FTIR maps of HAG + 5% wax + 5% PEG-iso and HAG + 10% wax + 5% PEG-iso films. These S-FTIR maps indicate the presence of wax and PEG-isocyanate by CH_2 and NH absorption intensity colour coded scales, respectively, across the thickness of these films. (The S-FTIR map of HAG + 10% CB + 5% PEG-iso film is not included due to cracked while drying.) (For interpretation of the references to color in this figure legend, the reader is referred to the web version of the article.)

crosslinking reaction between PEG-iso and starch molecules. Furthermore, the presence C=O (carbonyl stretching) peak between 1700–1740 cm^{-1} further corroborated the above results (Jyothi & Carvalho, 2013). The concentration of PEG-iso affected the peaks associated with the carbonyl stretching (1732 cm^{-1}) and C—N and N—H stretching (1532 cm^{-1}). As shown in Fig. 1B: a, b, c, j, k, l, the addition of 20% PEG-iso to the HAG + wax matrix showed strong peaks at 1732 cm^{-1} and 1532 cm^{-1}. These peaks decrease in relative intensity as the PEG-iso concentration decrease to 5% and 1%.

Based on the above observations, wavenumbers 2840 cm^{-1} and 1530 cm^{-1} were used in this study to identify the pattern of distribution of natural wax and PEG-isocyanate, respectively, across the thickness of these films. Fig. 2 presents the chemical map with colour codes to indicate the presence of wax calculated from the absorbance intensity of CH_2 stretching. The intensity scale and the

presence of PEG-iso calculated from the intensity scale of NH bending are also presented in Fig. 2. The HAG film was used as this film did not show CH_2 and NH absorption peaks as evident in Fig. 2. The SEM images and CA values of HAG and HAG + was films used from our earlier work for comparison purpose (Muscat et al., 2013).

All the cast films dried into flat films with some degree of curled edges. However, films of HAG + 10% CB + 5% PEG-isocyanate and HAG + 10% wax + 1% PEG-isocyanate showed intensive cracking during the drying step. Consequently, we did not analyze these films for their hydrophobicity, S-FTIR and SEM imaging and CA values.

3.2. The distribution of wax in HAG + wax films

The S-FTIR maps and CH_2 and NH absorption intensity values for HAG matrix in the presence of 5% BW, CL and CB (Fig. 2) show that these waxes were randomly distributed across the thickness of these films as seen in the chemical map of CH_2 absorption (2840 cm^{-1}). In a previous study (Muscat et al., 2014) it was suggests that at a concentration of 5% (w/w) these waxes crystallized at an earlier stage of the drying process within the composite films, i.e. before the completion of the film formation. This rapid crystallization caused these waxes to be randomly distributed within these films. Furthermore, the presence of 10% (w/w) concentration of these waxes allowed them to solidify into wax-rich domains in the middle of the dried HAG + wax films.

3.3. The distribution of wax and PEG-iso in HAG + wax + PEG-iso films

The distribution of wax and PEG-iso in HAG + wax + 20% PEG-iso, HAG + wax + 5% PEG-iso and HAG + wax + 1% PEG-iso films are shown in Figs. 3, 4 and 5, respectively.

The S-FTIR maps and CH_2 and NH absorption intensity values for 5% and 10% CB, CL, and BW and 20% PEG-iso films are shown in Fig. 3. It can be observed from this figure that the addition of 20% PEG-iso to the HAG + wax matrix influenced the distribution of the wax across the thickness of the film. The HAG + 5%CL + 20%PEG-iso film exhibited a distribution of CL as two wax-rich domains at either end of the film with a PEG-iso rich domain formed in the middle of this film. These CL wax-rich domains appear to be attached to the PEG-iso and have crystallized on either side of this film. The NH absorption value read 46.2 indicating a high concentration of PEG-iso in the middle of the film. At a concentration of 5%, CB and BW waxes crystallized differently in the presence of 20% PEG-iso. These waxes crystallized into a single wax-rich domain which progressively decreased towards the surface of these films. Because of this reason, the PEG-iso domain appeared to be positioned on either sides of the wax. The NH absorption value in these films was 27.2 and 33.1 suggesting a high presence of 20% PEG-iso at the surfaces of these films. It can be seen from Fig. 3 that the S-FTIR maps of 10% wax + 20% PEG-iso films formed distribution pattern similar to those films containing 5% wax + 20% PEG-iso. As can be observed from the S-FTIR maps, the films containing 10% CB and BW exhibited a single wax-rich domain in the middle of the films. The PEG-iso rich domains were formed either to the drying surface or in the middle of the films containing 20% PEG-iso. These different PEG-iso distribution patterns affected the NH absorption value of these films. When the PEG-iso was located at the drying surface of HAG + 10% CB + 20% PEG the NH absorption value was 45.1. The NH absorption value increased to 60.2 once the PEG-iso was positioned in the middle of HAG + 10% BW + 20% PEG-iso film. The 10% CL + 20% PEG-iso film showed two wax-rich bands at each end of the film with a high proportion of PEG-iso (NH absorption value of 14.5) present towards the surface of this film at which drying occurred.

In Fig. 4, the S-FTIR maps and CH_2 and NH absorption intensity values for 5% and 10% CB, CL, and BW and 5% PEG-iso films are shown. The 5% CB + 5% PEG-iso film show that the wax has preferentially located into wax-rich domains at the surfaces of this film. It appears that both the wax and PEG-iso had migrated to the surface of this film during drying. The S-FTIR map of 5% BW + 5% PEG-iso film showed that both the BW and PEG-iso were randomly distributed across the thickness of this film. In the case of 5% CL + 5% PEG-iso film, the S-FTIR map showed CL was randomly distributed in this film and the PEG-iso was attached to one side of these wax-rich bands. The 10% CL + 5% PEG-iso film exhibited a different distribution of CL and PEG-iso compared to other films. The S-FTIR maps of both CL and PEG-iso showed that these components had migrated towards the drying surface of the film to create a pinnacle point with a high concentration of CL and PEG-iso. This suggests that the water evaporation flux at the drying end of the film helped the migration of both CL and PEG-iso to produce a wax-rich surface. Then S-FTIR map of 10% BW + 5% PEG film suggested both the BW and PEG-iso were randomly distributed across the thickness of this film.

The S-FTIR maps and CH_2 and NH absorption intensity values for 5% CB, CL, and BW and 1% PEG-iso films are shown in Fig. 5. The 10% wax with 1% PEG-iso could not be analyzed owing to severe drying induced cracking of these films. As can be seen from this figure, the CB was distributed in the middle of the film and the PEG-iso rich band was positioned to the evaporating side of 5% CB + 1% PEG-iso film. When 1% PEG-iso was added to HAG + 5% CL, it was observed that the CL was found to migrate to one side of the film causing CL to form wax-rich domains towards the evaporating end of this film. However, PEG-iso was found to be distributed randomly across the film. This type of distribution was similarly displayed by HAG + 5% BW + 1% PEG-iso film.

3.4. Relationship between the hydrophobicity and the distribution of wax and PEG-iso

Figs. 2–5 show the S-FTIR maps and CH_2 and NH absorption intensity values for HAG + wax and HAG + wax + PEG-iso films. The contact angle values of these films are presented in Figs. 2 and 6–8 to determine the relationship between the hydrophobicity of the films with the distribution of wax within these films.

The contact angle value of the HAG film was the lowest at 43.3° compared to other films (Fig. 2). When natural waxes were incorporated into the HAG matrix to form HAG + wax films their CA values increased up to 65.6°. The observations of the S-FTIR maps presented in Fig. 2 helps explain why the addition of wax increases the CA values in HAG + wax films. The S-FTIR maps reveal that the wax component in these films were generally randomly distributed (e.g. at 5% concentration) or displayed a wax-rich domain in the centre region across the thickness of the film at 10% concentration. In a recent study, Muscat, Tobin, Guo, & Adhikari (2014) found that the pattern of wax distribution across the thickness of these films was responsible for the observed hydrophobicity (CA values) of the films. It was stated the addition of 5% wax caused recrystallization at an earlier stage of the drying process within these casted HAG + wax films. This occurred due to the optimized drying temperature of 20 °C was lower than the melting points of these natural waxes consequently encouraging rapid recrystallization, thus creating random wax distribution across these films. When the addition of these waxes was increased to 10%, wax-rich domains formed in the interior of these films. This observation suggested the increased wax concentration caused these waxes to recrystallize much faster. This implies that when wax forms a wax-rich domain there is an increase in surface roughness of the film as observed from the surface morphology (SEM images) of the HAG film. Although the presence of wax crystals on the surface

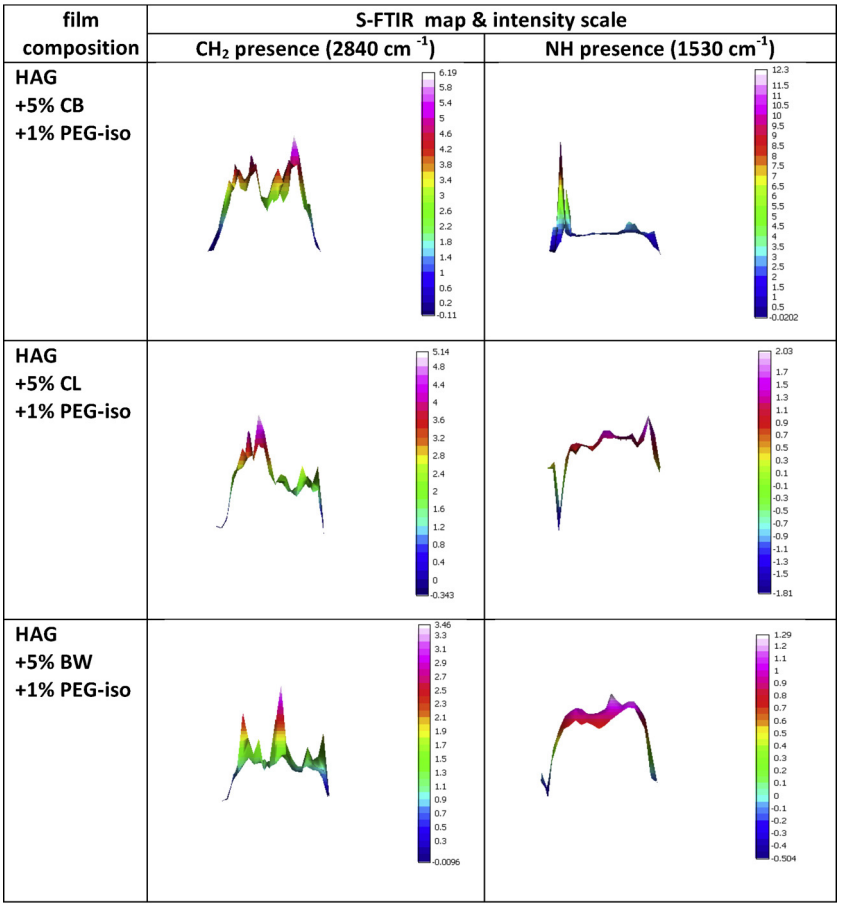

Fig. 5. The S-FTIR maps of HAG + 5% wax + 1% PEG-iso films. These S-FTIR maps indicate the presence wax and PEG-isocyanate by CH_2 and NH absorption instensity colour coded scales, respectively, across the thickness of these films. (The S-FTIR map of the HAG + 10% wax + 1% PEG-iso films are not included due to cracked while drying.) (For interpretation of the references to color in this figure legend, the reader is referred to the web version of the article.)

of the HAG matrix resulted in an increase in the surface roughness (Chung & Lai, 2005), the hydrophobic property of these waxes depends on the percentage and orientation of their constituents (Holloway, 1969).

The CA values and SEM micrographs for the HAG + 5% wax + PEG-iso and HAG + 10% wax + PEG-iso films at 20%, 5% and 1% PEG-iso are presented in Figs. 6, 7 and 8, respectively. The S-FTIR maps and CH_2 and NH absorption intensity values for the HAG + 5% wax + 20% PEG-iso and HAG + 10% wax + 20% PEG-iso films are presented in Fig. 3. The addition of 20% PEG-iso to HAG + 5% wax and HAG + 10% wax matrices caused these waxes to be distributed as wax-rich domains within the films. These wax-rich domains could be classified as a single broad domain towards the centre of the film or two domains towards the edge of either side of the film. It is essential that the distribution of wax and PEG-iso in these films is examined along with the CA values and SEM micrographs (Fig. 6) in order to explain the film hydrophobicity. When 20% PEG-iso was added to HAG + 5% CB film, this wax was distributed as a wax-rich domain towards the evaporating surface but the PEG-iso was distributed on either side of the film. This distribution pattern of PEG-iso had a NH absorption intensity value of 27.2. A similar distribution of wax-rich domains across the thickness of the film and higher NH absorption intensity value (33.1 and 14.50) of PEG-iso at the surface of the film were observed in HAG + 5%BW + 20%PEG-iso and HAG + 10% CL + 20% PEG-iso films and the CA values of these films are 66.6° and 64.9°, respectively which are not significantly different ($p > 0.05$). These increased CA values suggest that the incorporation of 20% PEG-iso to HAG + wax matrix increased the hydrophobicity of these films significantly (by 20°, $p < 0.05$). The S-FTIR maps of the films containing 20% PEG-iso in a HAG + wax matrix (Fig. 3) showed different distribution of wax and PEG-iso compared to the films observed above. Both the HAG + 5% CL + 20% PEG-iso and HAG + 10% BW + 20% PEG-iso films exhibited unique distribution of PEG-iso where PEG-iso rich domains were present in the middle of these films. The recrystallization of the waxes occurred as wax-rich domains at each end (i.e. surface) or as a single broad wax-rich domain in the middle of these films. This arrangement of wax and 20% PEG-iso resulted into the highest hydrophobicity with CA values of 90.4° and 91.8°, respectively. It can be observed from Fig. 3 that the films with high CA values had a high intensity of NH absorption value between 60.2 and 45.1. This suggests that the synergistic interaction of PEG-iso in the middle of the film with HAG + wax significantly ($p < 0.05$) increased the degree of hydrophobicity (increase of CA by 30°). The distribution of wax and 20% PEG-iso was differently observed in HAG + 10%CB + 20%PEG-iso film as the wax and PEG-iso were both distributed on the surface of this film. Although the NH absorption intensity value was high at 45.1 the presence of PEG-iso on the surface caused the CA value to marginally decrease to 83.1°.

The S-FTIR maps and CH_2 and NH absorption intensity values for the HAG + 5% wax + 5% PEG-iso and HAG + 10% wax + 5% PEG-iso films are presented in Fig. 4. The corresponding CA values of these films are presented in Fig. 7. The CA values of these films likewise correlate to the distribution of wax and 5% PEG-iso across the thickness of these films. The HAG + 5% CB + 5% PEG-iso film displayed a S-FTIR map where wax-rich domains were positioned at the surface-end of the film and a PEG-iso-rich domain was present on the surface. When 5% PEG-iso was introduced to HAG + 5% CL the

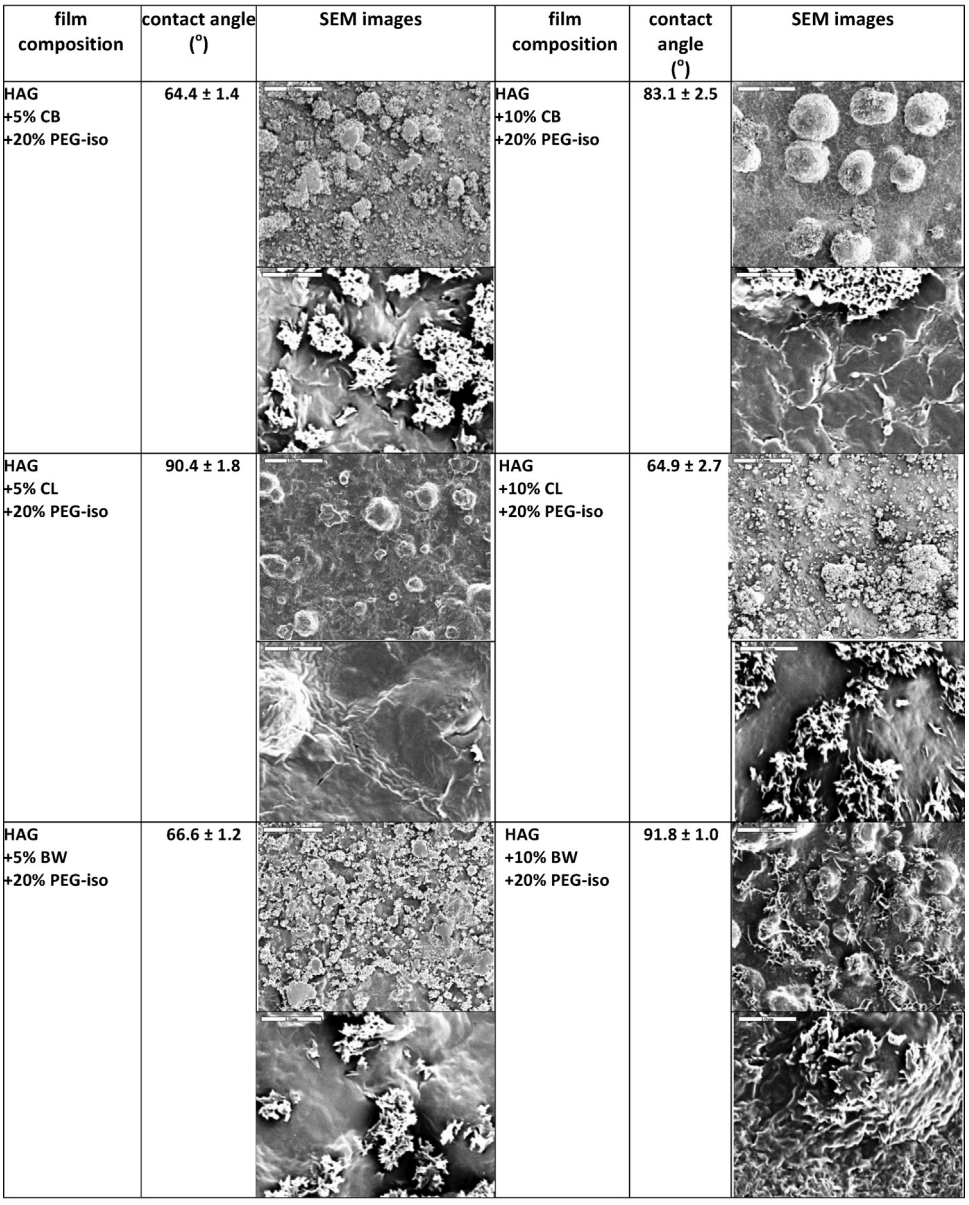

Fig. 6. SEM images, 100 μm (above) and 10 μm (below) and CA values of HAG + wax + 20% PEG-iso films.

distribution of CL and PEG-iso revealed quite different pattern. In this film, the wax-rich domains were distributed to both the drying end and non-drying end surfaces of the film and a PEG-iso-rich band was observed towards the drying end of the surface. This pattern of distribution resulted in a CA value of 79.3°. The addition of 5% PEG-iso to 5% CB created a similar wax and PEG-iso distribution pattern and had a CA value of 65.0°. Yet another wax and PEG-iso distribution pattern was observed when 5% PEG-iso was added to 5% and 10% BW + HAG matrices. At both these concentrations the PEG-iso and BW were randomly distributed across the thickness of the film. The random distribution of wax and PEG-iso resulted in low CA values of 50.8° and 55.6°. Interestingly, the addition of 5% PEG-iso to HAG + 10% CL caused the CL to recrystallize into multiple pinnacle points towards the evaporation surface of this film. Relatively high NH absorption intensity value was observed at this evaporating end of this film causing an increase in CA value (86.0°).

The S-FTIR maps and CH_2 and NH absorption intensity values for the HAG + 5% wax + 1% PEG-iso films are presented in Fig. 5 and their corresponding CA values are presented in Fig. 8. The 5% wax + 1% PEG-iso films generally formed two different patterns of distribution of wax and PEG-iso. It was observed that wax-rich domains were formed towards the surface of films containing 5% of CL and CB. Both of these films showed that the PEG-iso was distributed at the drying surface of these films. This pattern of distribution of wax and PEG-iso in 5% wax and 1% PEG-iso resulted in CA values of 73.5° and 78.3° for CB and CL, respectively. In the case of HAG + 5% BW + 1% PEG-iso film, both the wax and PEG-iso were found to be randomly distributed across the thickness of the film consequently resulting into a low CA value (54.4°).

The above observations relating to the distribution of wax and PEG-iso across the thickness of the films and the corresponding CA values indicate that there is a correlation between these two factors. The CA values of these films can be grouped into five distinct ranges: >90°, 80–89°, 70–79°· 60–69°, and 50–59° (Figs. 6–8). Each of these CA value ranges are related to the particular pattern of distribution of wax and PEG-iso across the thickness of these films (Figs. 3–5). It appears that when the PEG-iso-rich domain (NH absorption chemical intensity value was greater than 46) was present towards the

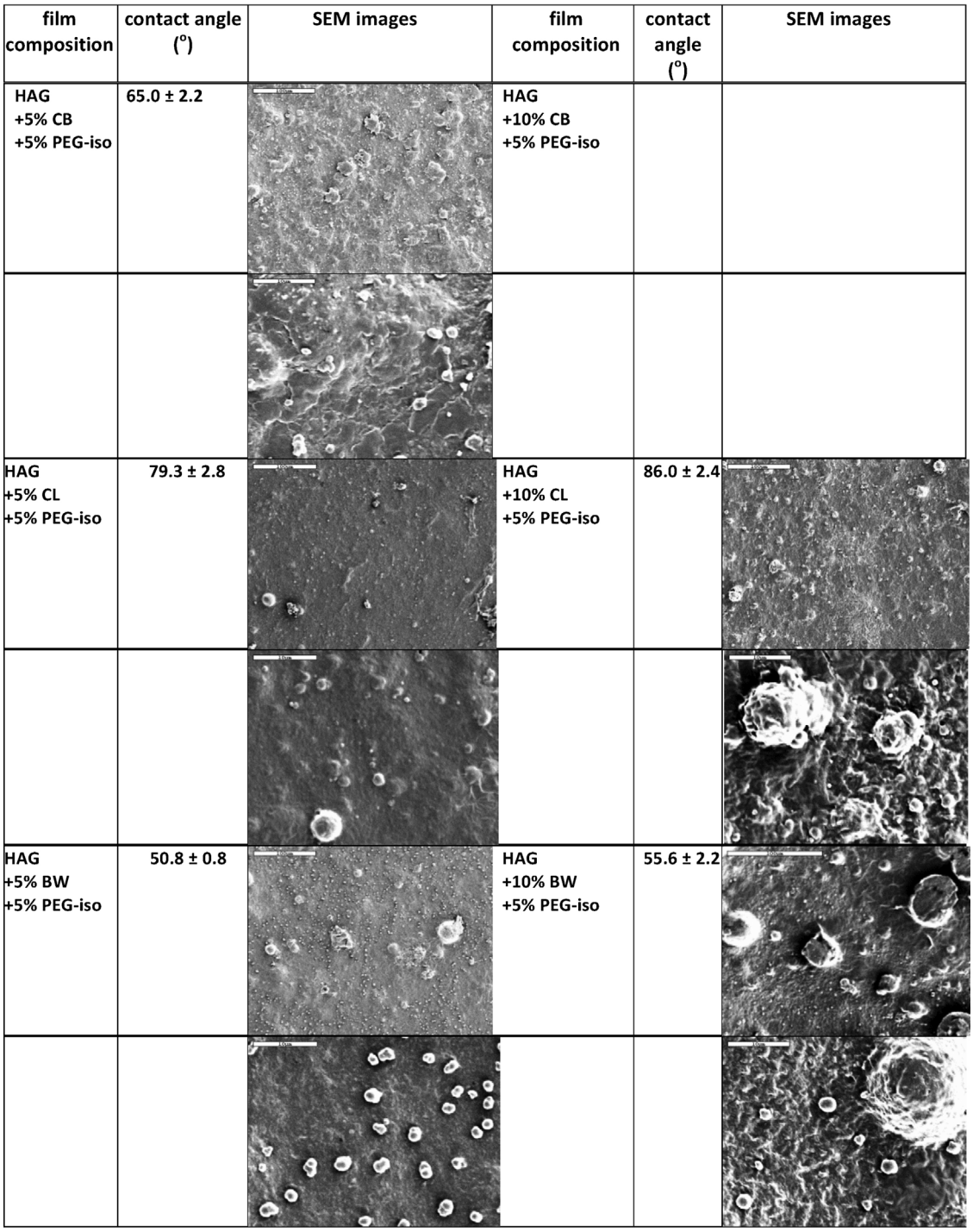

Fig. 7. SEM images, 100 μm (above) and 10 μm (below) and CA values of HAG + wax + 5% PEG-iso films. (The SEM image of HAG + 10% wax + 5% PEG-iso film is not included due to cracked while drying.)

middle of the film, and also accompanied with wax-rich domains towards the drying-end surface or towards the middle of the film, the resultant CA value is greater than 90°. This signifies that the wax is attached to the HAG matrix by PEG-iso, creating a layer of wax onto the HAG thereby increasing the hydrophobicity. The HAG + 5% CL + 20% PEG-iso and HAG + 10% BW + 20% PEG-iso films showed CA values in this range. Another wax and PEG-iso distribution pattern was observed when both these components seemingly created multiple pinnacle points towards the surface of the film at which the drying occurred in the S-FTIR maps. These maps seem to suggest that both the wax and PEG-iso migrated to the evaporating surface during drying forming relatively rich domains of both wax and PEG-iso. This type of pattern was observed in HAG + 10% CL + 5% PEG-iso and HAG + 10% CB + 20% PEG-iso films which had CA values in the 80–89° range. Another distinct distribution of wax and PEG-iso was observed across these films where the wax-rich and the PEG-iso rich domains were formed on the drying surface of these films. The presence of PEG-iso on the film surface appears to interfere with the hydrophobic characteristics of these waxes and lowers the CA values of these films between 70–79°. The films which had 5% and 1% PEG-iso in their composition had minimal interference with the characteristics of the wax. The films with

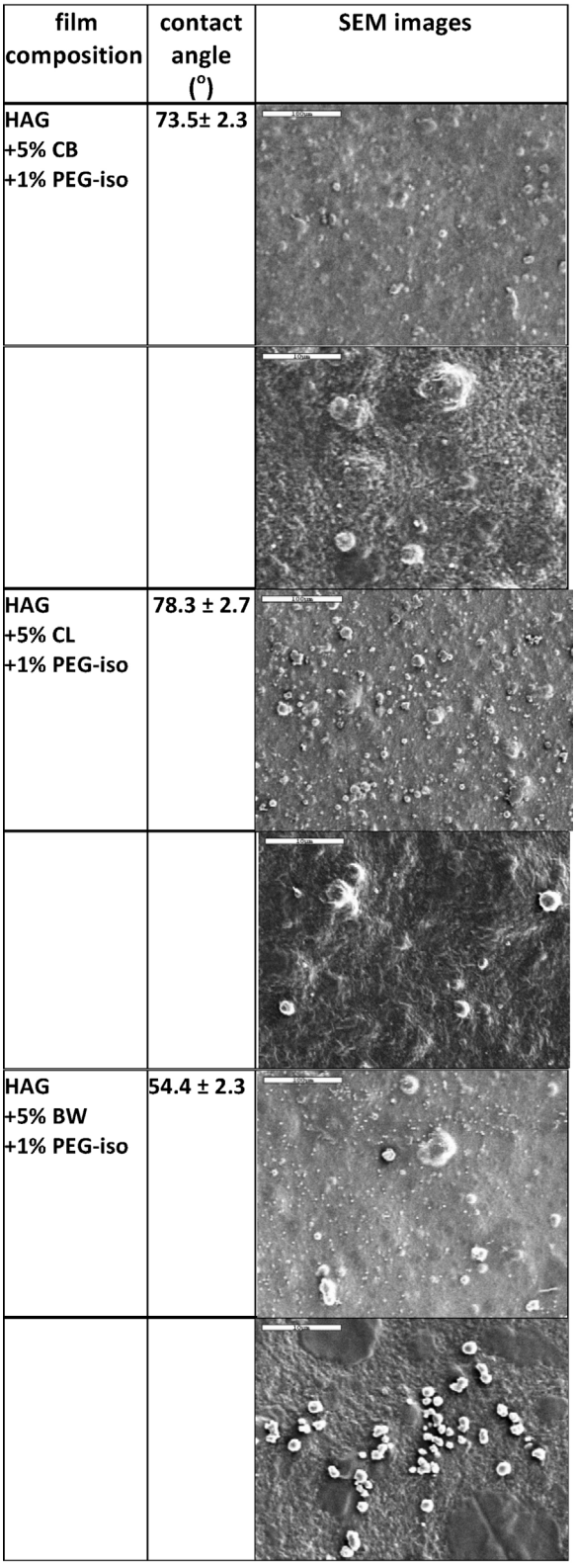

Fig. 8. SEM images, 100 μm (above) and 10 μm (below) and CA values of HAG + wax + 1% PEG-iso films. (The SEM images of HAG + 10% wax + 1% PEG-iso films are not included due to cracked while drying.)

this type of distribution pattern were HAG + 5% CB + 1% PEG-iso, HAG + 5% CL + 1% PEG-iso and HAG + 5% CL + 1% PEG-iso films which had CA values of 79.3°, 73.5°, and 78.3°, respectively. The films having wax-rich and PEG-iso rich domains towards the middle or on the films surfaces had CA values in the range of 60–69°. The distribution of PEG-iso on the film surface with or without the presence of wax greatly affected the hydrophobicity of the films. This influence was greater in the films which had 20% PEG-iso. The NH absorption value of films containing 20% PEG-iso was in the range of 14 to 35 indicating a greater effect of PEG-iso at this concentration. The films in this category were HAG + 5% CB + 20% PEG-iso, HAG + 5% BW + 20% PEG-iso, and HAG + 10% CL + 20% PEG-iso which had CA values of 64.4°, 66.6°, and 64.9°, respectively. A notable exception was the HAG + 5% CB + 5% PEG-iso film which had a CA value of 65.0°; albeit it had only 5% PEG-iso. The lowest range of CA values (50–59°) was observed in the films in which the wax and PEG-iso were randomly distributed across the thickness of these films. This pattern of wax distribution was formed when the wax was recrystallised at an early stage of film drying (Muscat, Tobin, Guo, & Adhikari, 2014). The early crystallization of wax means that it could not migrate to the surfaces of the film as desired. The PEG-iso in this formulation also showed random distribution suggesting that it was attached to the wax. The films which exhibited the CA values in the lowest range were HAG + 5% BW + 5% PEG-iso (50.8°), HAG + 10% BW + 5% PEG-iso (55.6°), and HAG + 5% BW + 1% PEG-iso (54.4°).

The above observations suggest that the S-FTIR maps can be utilized to obtain better understanding of the hydrophobicity of these films. The S-FTIR maps helped explain the effect of the nature and concentration of natural waxes on the distribution across the thickness of the films. The S-FTIR maps help explain how the distribution patterns of wax and PEG-iso affect the surface hydrophobicity in HAG + wax and HAG + wax + PE-iso films. The S-FTIR maps have demonstrated that when PEG-iso was positioned in the middle of these films rather than on the surface had generated hydrophobic films with CA values greater than 90°.

3.5. *Effect of the distribution of wax and PEG-iso on the film surface morphology*

The SEM micrographs of HAG, HAG + wax and HAG + wax + PEG-iso films are presented in Figs. 2, 6–8, respectively. These SEM images show the surface morphology of the studied films at 100 μm and at 10 μm resolution. As can be seen from these SEM images, the HAG film (Fig. 2) had a smoother surface compared to other films. The surface of the HAG + wax films were rougher compared to that of the HAG film. This rough surface was created by aggregation of wax droplets and subsequent recrystallization during film drying. The S-FTIR maps help explained the fact that the random distribution of these natural waxes within these films contributed to the increased surface roughness in HAG + wax films.

From the CA values and the SEM images (Figs. 6–8), it can be observed that the CA value is directly correlated with the surface morphology (i.e. roughness) of these films. The introduction of 20% PEG-iso to the HAG + wax films resulted in different types of surface morphology (Fig. 5). These SEM images bear resemblance to the S-FTIR maps at CH_2 and NH absorptions where the surface of these films is occupied by different components. The surface morphology of HAG + 5% CB + 20% PEG-iso, HAG + 5% BW + 20% PEG-iso and HAG + 10% CL + 20% PEG-iso films is similar indicating that the chemical composition of these films is almost identical. The distribution of HAG, wax and PEG-iso in these films created a hierarchical coral like structure extending upwards from the texturized surface featuring pits and bumps on these films. As shown in Fig. 3 the PEG-iso-rich domains were arranged at the surface of these films with a wax-rich domain in the middle or on the surfaces. The wax had crystallized on the surface to form this coral like surface morphology. It appears the coral like formation was the wax component of the film. The HAG + 5% CL + 20% PEG-iso, HAG + 10% CB + 20% PEG-iso and HAG + 10% BW + 20% PEG-iso films showed different surface morphology which comprised of raised circular pinnacle structures embedded on a textured surface

featuring pits and bumps. When a careful observation of these SEM images together with their corresponding S-FTIR maps is made; it appears that the raised circular pinnacle structures were made up of recrystallized wax domains. The diameter of these circular structures appeared to influence the CA values attained by these films. The formation of 10 μm diameter hierarchical circular pinnacle wax structure caused the CA values of HAG + 5% CL + 20% PEG-iso and HAG + 10% BW + 20% PEG-iso films to increase to a hydrophobic level (> 90°). The surface morphology of HAG + 10% BW + 20% PEG-iso film appeared to have extra fine threads adjoining the recrystallized wax which also caused the CA value to increase. Although HAG + 10% CB + 20% PEG-iso film displayed raised circular pinnacle structures, the diameter of these structures was larger than 10 μm which seemed to marginally impact on the CA value (decrease to 83.1°). The other noteworthy factor which seems to increase the CA value up to the hydrophobic level is the distance between these (recrystallized) wax circular structures. As shown in Fig. 6, the closer the distance of these raised circular pinnacle structures the higher the CA value.

The surface morphology of HAG + 5% wax + 5% PEG-iso and HAG + 10% wax +5% PEG-iso films (Fig. 7) show that the formation of a less complex structures which lowered the CA value. The decrease in the concentration of PEG-iso and NH absorption intensity value in these HAG + wax films decreased their CA values. The films which had the CA value in the range of 50–59° apparently had a smoother surface with numerous smaller circular formations ranging below 1 μm speckled over the film surface resulting in low CA values in HAG + 5% BW + 5% PEG-iso (50.8°) and HAG + 10% BW + 5% PEG-iso (55.6°) films. As discussed earlier, the S-FTIR maps of these films showed that the wax and PEG-iso were randomly distributed across the thickness of these films suggesting that there was less wax and PEG-iso on the surface of these films. The wax attached with PEG-iso recrystallized in the early stage of drying, and hence, the wax and PEG-iso could not migrate to the film surface to create wax-rich hydrophobic domains, instead these components were distributed randomly across the film. The HAG + 5% CB + 5% PEG-iso film showed a different SEM image and lower CA values compared to the films containing 20% PEG. The SEM image of this film showed a textured surface with raised circular structures (approximately 1 μm) of both CB and PEG-iso disturbed on the surface of this film. The SEM image of HAG + 10% CL + 5% PEG-iso film showed numerous raised circular structures (diameter <10 μm) embedded on a textured surface featuring pits and bumps. These structures were responsible for increasing the CA to 86°. The SEM image of HAG + 5% CL + 5% PEG-iso film had a similar textured surface with the presence of smaller circular raised wax crystals on the surface of this film. This observation was corroborated by the S-FTIR map which showed that a substantial amount of CL was present on the surfaces of this film along with the PEG-iso generating a CA value of 79.3°.

The SEM images and CA values HAG + 5% wax + 1% PEG-iso films are shown in Fig. 8. The relationships among the distribution of wax and PEG-iso, the surface morphology (SEM images) and the surface hydrophobicity (CA values) of these films were similar to those observed in HAG + wax + 5% PEG-iso films as discussed earlier.

The dependence of hydrophobicity of these films to their surface morphology and properties of the epicuticular wax can be explained in terms of the amount of air spaces observed in the nanoscale in an earlier work by Ensikat, Ditsche-Kuru, Neinhuis, & Barthlott (2011). According to these authors, the wax crystals and additional hierarchical surface structures such as papillae help in trapping the air in the film surface. The morphology of the papillae with small tip minimizes the contact area to the water drops. Thus, the film which entraps a relatively large volume of air shows higher hydrophobic characteristics (Subedi, Madhup, Sharma, Joshi, & Huczko, 2012). This is evident in our observations (Fig. 6) especially in HAG + 5% CL + 20% PEG-iso and HAG + 10% BW + 20% PEG-iso films. These films showed CA values of 90.4° and 91.8°, respectively, which can be attributed to the high volume of air trapped in these films due to the hierarchical circular pinnacle wax structure on the textured surface on these films.

4. Conclusions

The S-FTIR maps and chemical intensity scale provided valuable information regarding the distribution of wax and PEG-iso across the thickness of the HAG + wax + PEG-iso films. The S-FTIR maps of the HAG + wax + PEG-iso films showed a number of spatial distribution patterns of wax and PEG-iso as well as a number of crystallization patterns of wax in these films. Both the SEM images and the S-FTIR maps showed that the distribution pattern and especially the migration and crystallization of wax on the film surface significantly ($p < 0.05$) affected the surface morphology and surface hydrophobicity of these films. The hydrophobicity of the films was highest when the wax-rich domains were distributed either in the middle of the films or on the surface and the PEG-iso rich domains were distributed in the middle of these films. This spatial distribution pattern of wax and PEG-iso was found to result in the highest hydrophobicity (contact angle >90°). The HAG + wax + PEG-iso films having the highest hydrophobicity also displayed a very sophisticated hierarchical circular pinnacle structure of solidified wax on the film surface which were attached with PEG-iso. The recrystallized wax which formed approximately 10 μm raised circular structures in close proximity with each other and adjoined with fine threads on a textured surface were found to be responsible for the very high hydrophobicity. The S-FTIR maps, contact angle and the SEM images were found to be helpful in providing the correlation between the spatial distribution of wax, the surface morphology and the surface hydrophobicity these films.

Acknowledgements

We wish to thank the Australian Synchrotron management (Clayton, VIC, Australia) for allowing us to use the S-FTIR beamline. We also wish to thank our colleagues Dr Huihua Liu and Dr Amir Ghandi for their assistance with the preparation of the film window.

References

Borona, G. M., & Drioli, S. (2009). Reactive PEGs for protein conjugation. In F. M. Veronese (Ed.), *PEGylated protein drugs: Basic science and clinical applications* (pp. 33–45). Switzerland: Birhause Verlag.

Brittain, W. J., & Minko, S. (2007). Highlight: A structural definition of polymer brushes. *Journal of Polymer Science Part A: Polymer Chemistry*, *45*, 3505–3512.

Brugnara, M. (2006). *Contact Angle Plugin (for ImageJ software)*. Available at: http://rsbweb.nih.gov/ij/plugins/contact-angle.html (accessed on: July, 2011)

Chechik, V., Crooks, R. M., & Stirling, C. J. M. (2000). Reactions and reactivity in self-assembled monolayer. *Advanced Materials*, *12*, 1161–1171.

Coates, J. (2000). Interpretation of infrared spectra, a practical approach. In R. A. Meyers (Ed.), *Encyclopedia of analytical chemistry* (pp. 10815–10837). Chichester, UK: John Wiley & Sons Ltd.

Chung, Y., & Lai, H. (2005). Water-barrier property of starch films investigated by magnetic resonance imaging. *Cereal Chemistry*, *82*(2), 131–137.

de Vlieger, J. J. (2003). Chapter 24: Green plastic for food packaging. In R. Advenainen (Ed.), *Novel food packaging techniques* (pp. 519–534). Cambridge, England: Woodhead Publishing Limited.

Ensikat, H. J., Boese, M., Mader, W., Barthlott, W., & Koch, K. (2006). Crystallinity of plant epicuticular waxes: Electron and X-ray diffraction studies. *Chemistry and Physics of Lipids*, *144*, 45–59.

Ensikat, H. J., Ditsche-Kuru, P., Neinhuis, C., & Barthlott, W. (2011). Superhydrophobicity in perfection: The outstanding properties of the lotus leaf. *Beilsten Journal Nanotechnology*, *2*, 152–161.

Fink, J. K. (2011). . *Handbook of engineering and specialty thermoplastics: Water soluble polymers* (Vol. 2) Hoboken, NJ, USA: John Wiley and Sons, Inc. Chapter 1 – Poly(ethylene oxide).

Guelcher, S. A., Gallagher, K. M., Didier, J. E., Klinedinst, D. B., Doctor, J. S., & Goldstein, A. S. (2005). Synthesis of biocompatible segmented polyurethanes from aliphatic diisocyanates and diurea diol chain extenders. *Acta Biomaterialia*, *1*, 471–484.

Han, J. H., & Gennadios, A. (2005). *Edible films and coatings: A review. Innovations in food packaging. Food science and technology international series* London: Elsevier.

Harris, J. M. (1992). Chapter 1: Introduction to biotechnical and biomedical applications of poly(ethylene glycol). In J. M. Harris (Ed.), *Poly(ethylene glycol) chemistry: Biotechnical and biomedical applications* (pp. 1–14). New York: Plenum Press.

Hermanson, G. T. (2008). *Bioconjugate techniques* (2nd ed.). CA, USA: Academic Press.

Holloway, P. J. (1969). Chemistry of leaf waxes in relation to wetting. *Journal of the Science of Food and Agriculture*, *20*(2), 124–128.

Howard, G. T. (2002). Biodegradation of polyurethane: A review. *International Biodeterioration & Biodegradation*, *49*, 245–252.

Iheagwara, M. C. (2013). Isolation, modification and characterization of sweet potato (*Ipomoea batatas* L (Lam)) starch. *Journal of Food Process and Technology*, *4*(1), 1000198, 1–6.

Jetter, R., & Kunst, L. (2008). Harnessing plant biomass for biofuels and biomaterials: Plant surface lipid biosynthetic pathways and their utility for metabolic engineering of waxes and hydrocarbon biofuels. *Plant Journal*, *54*, 670–683.

Jyothi, A. N., & Carvalho, A. J. F. (2013). Starch-g-copolymers: Synthesis, properties and application. In S. Kalia, & M. W. Sabaa (Eds.), *Polysaccharide based grafted copolymers* (pp. 59–109). Berlin, Heidelberg: Springer-Verlag.

Koch, K., & Ensikat, H.-J. (2008). The hydrophobic coatings of plant surfaces: Epicuticular wax crystals and their morphologies, crystallinity and molecular self-assembly. *Micron*, *39*, 759–772.

Kumar, G. T., Prakash, N. J., Laxmi, N., & Krishma, T. D. (2011). Biotechnology based drug delivery by PEGylation method. *International Journal of Research in Ayurveda and Pharmacy*, *2*(1), 95–102.

Lin, N., Huang, J., Chang, P. R., Anderson, D. P., & Yu, J. (2011). Preparation, modification and application of starch nanocrystals in nanomaterials: A review. *Journal of Nanomaterials*, *2011*, 1–13.

Marmur, A. (2004). The lotus effect: Superhydrophobicity and metastability. *Langmuir*, *20*, 3517–3519.

Miller, L. M. (2002). *Infrared microspectroscopy and imaging*. Available at: http://www.bnl.gov/ps/nsls/newsroom/publications/otherpubs/imaging/workshopmiller.pdf (accessed on: July, 2011)

Muscat, D., Adhikari, B., Adhikari, R., & Chaudhary, D. S. (2012). Comparative study of film forming behaviour of low and high amylose starches using glycerol and xylitol as plasticizers. *Journal of Food Engineering*, *109*, 189–201.

Muscat, D., Adhikari, R., McKnight, S., Guo, Q., & Adhikari, B. (2013). The physicochemical characteristics and hydrophobicity of high amylose starch and glycerol films in the presence of three natural waxes. *Journal of Food Engineering*, *119*(2), 205–219.

Muscat, D., Tobin, M., Guo, Q., & Adhikari, B. (2014). Understanding the distribution of natural wax in starch-wax films using Synchrotron-based FTIR. *Carbohydrate Polymers*, *102*, 125–135.

Oles, M., Nun, E., Dambacher, G., & Schleich, B. (2000). Learning from nature – Polymer surfaces with a nano structure that utilise the Lotus-effect and clean themselves. In E. A. Dittmar, & D. Beebe (Eds.), *Ist annual international IEEE-EMBS special topic conference on microtechnologies in medicine and biology. Proceedings IEE ENEW YORK* (pp. 331–333).

Park, J. W., Im, S. S., Kim, S. H., & Kim, Y. H. (2000). Biodegradable polymer blends of poly (L-lactic acid) and gelatinized starch. *Polymer Engineering and Science*, *40*(12), 2539–2550.

Pereira, A. G. B., Paulino, A. T., Rubira, A. F., & Muniz, E. C. (2010). Polymer–polymer miscibility in PEO/cationic starch and PEO/hydrophobic starch blends. *EXPRESS Polymer Letters*, *4*(8), 488–499.

Prajapati, S. T., Patel, A. N., & Patel, C. N. (2011). Pegylation: An approach for protein and petptide drug delivery systems. *International Journal of Advance in Pharmaceutical Research (IJAPR)*, *2*(6), 252–262.

Roizard, D., Nilly, A., & Lochon, P. (2001). Preparation and study of crosslinked polyurethane films to factionate toluene-η-heptane mixtures by pervaportation. *Separation and Purification Technology*, *22-23*, 45–52.

Rasband, W. S. (2012). *ImageJ*. Bethesda, USA: U.S. National Institutes of Health. http://rsb.info.nih.gov/ij/index.html (accessed on: July, 2011)

Rhodes, A., Sandhu, S. S., & Onis, S. J. (2011). Chapter 2 – Surface modification of biomaterials by covalent binding of PEG. In R. Williams (Ed.), *Surface modification of biomaterials: methods, analysis and application* (pp. 39–55). Cambridge, UK: Woodhead Publishing Ltd.

Ruhe, J. (2004). Chapter 1 – Polymer brushes: On the way to tailer-made surfaces. In R. C. Advincula, W. J. Brittain, K. C. Caster, & J. Ruhe (Eds.), *Polymer brushes: Synthesis, characterization, applications* (pp. 1–33). Weinheim, Germany: WILEY-VCH Verlag GmbH & Co.

Stuart, B. H. (2004). Chapter 7 – Biological applications. In *Infrared spectroscopy: Fundamentals and applications*. Chichester, England: John Wiley & Sons Ltd.

Subedi, D. P., Madhup, D. K., Sharma, A., Joshi, U. M., & Huczko, A. (2012). Retracted: Study of the wettability of ZnO nanofilms. *International Nano Letters*, *2*, 1.

Tezcaner, A., & Hasirce, V. (2004). Chapter 9: Surface properties of polymeric biomaterials and their modification for tissue engineering applications. In M. Yaszemski, D. J. Trantolo, K.-L. Lewandrowski, V. Hasirci, D. E. Altobelli, & D. L. Wises (Eds.), *Tissue engineering and novel delivery system* (pp. 173–196). NY, USA: Marcel Dekker.

Torchilin, V. P. (2010). Chapter 26: Multifunctional pharmaceutical nanocarriers. In K. D. Sattler (Ed.), *Nanomedicine and nanorobotics* (pp. 26.1–26.26). Boca Raton, FL, USA: Taylor & Francis Group.

Veronese, F. M. (2001). Peptide and protein PEGylation: A review of problems and solutions. *Biomaterials*, *22*, 405–417.

Wagner, P., Furstner, R., Barthlott, W., & Neinhuis, C. (2003). Quantitative assessment to the structural basis of water repellency in nature and technical surfaces. *Journal of Experimental Botany*, *54*, 1295–1303.

Weetall, H. H. (1993). Preparation of immobilized proteins covalently coupled through silane coupling agents to inorganic supports. *Applied Biochemistry Biotechnology*, *41*, 157–188.

Williams, D. L., Kuhn, A. T., Amann, M. A., Hausinger, M. B., Konarik, M. M., & Nesselrode, E. I. (2010). Computerized measurement of contact angles. *Galvanotechnik*, *101*(11), 2502–2512.

Yiu, P. H., Loh, S. L., Rajan, A., Wong, S. C., & Bong, F. C. J. (2008). Physiochemical properties of sago starch modified by acid treatment in alcohol. *American Journal of Applied Sciences*, *5*, 307–311.

Yu, P. (2004). Horizons in nutritional science: Application of advanced synchrotron radiation-based Fourier transform infrared (SR-FTIR) microspectroscopy to animal nutrition and feed science: A novel approach. *British Journal of Nutrition*, *92*, 869–885.

Yu, P. (2012). Board-invited review: Sensitivity and responses of functional groups to feed processing methods on a molecular basis. *Journal of Animal Science and Biotechnology*, *3*, 40.

Zhang, Y., & Han, J. H. (2006). Plasticization of pea starch films with monosaccharides and polyols. *Journal of Food Science*, *71*(6), E253–E261.